Isochemical control over structural state and mechanical properties in Pd-based metallic glass by sputter deposition at elevated temperatures

Daniel J. Magagnosc, Gang Feng, Le Yu, Xuemei Cheng, and Daniel S. Gianola

---

Articles you may be interested in

Influence of the shot-peening intensity on the structure and near-surface mechanical properties of Ti40Zr10Cu38Pd12 bulk metallic glass
Appl. Phys. Lett. **103**, 211907 (2013); 10.1063/1.4833017

Patterned superhydrophobic surface based on Pd-based metallic glass
Appl. Phys. Lett. **101**, 081601 (2012); 10.1063/1.4747327

Nanoscale wavy fracture surface of a Pd-based bulk metallic glass
Appl. Phys. Lett. **94**, 131906 (2009); 10.1063/1.3109797

Thermal activation in Au-based bulk metallic glass characterized by high-temperature nanoindentation
Appl. Phys. Lett. **90**, 061911 (2007); 10.1063/1.2459383

Structural influence on atomic hopping and electronic states of Pd-based bulk metallic glasses
Appl. Phys. Lett. **86**, 072104 (2005); 10.1063/1.1866217

Isochemical control over structural state and mechanical properties in Pd-based metallic glass by sputter deposition at elevated temperatures

Daniel J. Magagnosc,[1] Gang Feng,[2] Le Yu,[3,4] Xuemei Cheng,[3] and Daniel S. Gianola[1,5,a]

[1]*Department of Materials Science and Engineering, University of Pennsylvania, Philadelphia, Pennsylvania 19104, USA*
[2]*Department of Mechanical Engineering, Villanova University, Villanova, Pennsylvania 19085, USA*
[3]*Department of Physics, Bryn Mawr College, Bryn Mawr, Pennsylvania 19010, USA*
[4]*School of Electronic Science and Engineering, Nanjing University, Nanjing 210093, China*
[5]*Materials Department, University of California, Santa Barbara, California 93106, USA*

Sputter deposition, while varying the substrate temperature, is employed to isochemically control the structural state and concomitant mechanical response in a Pd-based metallic glass at the time of glass formation. Increasing the deposition temperature from 333 K to 461 K results in a 33.5% increase in hardness to 9.69 GPa for amorphous films. Further increasing the temperature leads to a decrease in hardness, indicating low and high temperature deposition regimes where increased surface mobility allows access to a more relaxed and more rejuvenated structure, respectively. Through this mechanism we access the range of achievable structural states, from ultrastable to highly liquid-like glasses. © *2016 Author(s). All article content, except where otherwise noted, is licensed under a Creative Commons Attribution (CC BY) license (http://creativecommons.org/licenses/by/4.0/).* [http://dx.doi.org/10.1063/1.4960388]

Metallic glasses (MGs) are a unique class of materials, which exhibit many favorable properties including high strength and elastic strain limit owing to the combination of metallic bonding and amorphous structure.[1] However, MGs exhibit a distinct processing sensitivity owing to their inherent metastability. Rather than abruptly solidifying from the supercooled liquid like their crystalline counterparts, MGs smoothly transition from liquid to solid, leading to a continuous spectrum of packing polyhedral building blocks, with different populations of topological and chemical order, where slow cooling favors full icosahedra and fast cooling produces distorted polyhedra.[2] Yet, experimentally characterizing this range of glass structures through scattering methods remains largely intractable.[3] Conversely, physical properties, such as the excess enthalpy near the glass transition, provide clear delineation between different glass histories,[4] implying that subtle differences in glassy packing control macroscopically quantifiable properties.

History effects on glass structure result in many processing dependent properties. For instance, the mechanical properties are varied by changing the cooling rate,[5,6] annealing,[7,8] severe plastic deformation (SPD),[9–11] surface peening,[12–14] cyclic loading,[15–17] and ion irradiation.[18–20] The resulting changes in glass structure and properties can be classified as producing a relaxed or rejuvenated structure. Relaxed structures exhibit lower excess enthalpies[4] and increased hardness and modulus;[21,22] rejuvenated structures have large excess enthalpies and show lower hardness and modulus.[23]

While this conceptual framework provides a simple mapping of the glass structural state on a reduced energy spectrum, the details of the potential energy landscape (PEL), such as the mega-basin profile as well as the density and organization of inherent states, ultimately define the

---

[a]Email: gianola@engr.ucsb.edu

4, 086104-1

dynamical response of the glass. Some features of the PEL are sensitive to history effects while others are not.[24,25] However, quantification of the PEL or direct comparison of excess enthalpies is challenging given the diverse relaxation responses and differences in heat capacity.[26,27] Instead, the fictive temperature (T_f), which describes the temperature at which a structure would be at equilibrium, is readily determined from a calorimetric measurement of the heat capacity.[28] Furthermore, T_f is a powerful metric for quantifying MG structures and offers a facile comparison of different glasses and processing routes.[29]

Despite the advances in understanding the interplay between processing, structure, and properties in MGs, post-glass forming treatments dominate efforts to control mechanical properties in MGs, and the bounds of structural state are yet to be established. Conversely, control over structural state in organic glasses during glass formation has been achieved through physical vapor deposition (PVD).[30,31] By varying the deposition temperature, the structural state, as indicated by T_f, and material properties are controlled.[30–32] Additionally, a unique glassy state with exceptionally low T_f and enhanced stability, coined an ultrastable glass, was produced in organic glasses and thin film MGs,[33] as a result of enhanced surface mobility enabling adatoms to diffuse to a lowest energy disordered configuration.[34] While the ultrastable glass is likely the lowest energy bound on structural state, highly liquid-like structures may also be produced by PVD owing to effective cooling rates far greater than conventional thermal processing; this full spectrum of structural states has not been investigated in PVD thin film MGs. Furthermore, a detailed understanding of how mechanical properties change across the full range of structural states is still needed. Therefore, based on the isochemical control over structural state, PVD deposition of thin film MGs is proposed as a method to tailor the hardness and modulus at the time of glass formation rather than through tailoring alloy composition or post-glass forming treatments.

Here, we employed temperature-controlled DC magnetron sputtering to deposit $Pd_{77.5}Cu_6Si_{16.5}$ MG thin films from an alloy target. The target was produced from elemental sources with 99.99% (Pd source) and 99.999% (Cu and Si source) purity. Approximately 200 nm thick films were deposited in an AJA magnetron sputtering system at a working Ar pressure of 4 mTorr, a target power of 125 W, and a chamber base pressure of $<5 \times 10^{-8}$ Torr. The structural state was controlled during deposition by varying the substrate temperature via a quartz lamp heater. The substrate temperature was calibrated using irreversible temperature sensitive dots (Omega Label). Thus, all reported temperatures correspond to the actual growth temperature and not the set-point temperature. Thin film composition was verified by energy dispersive X-ray spectroscopy (EDS), which was cross-validated by Rutherford backscatter spectroscopy measurements on thin films deposited under similar conditions. X-ray diffraction (XRD) and transmission electron microscopy (TEM) were employed to verify the glassy structure. Mechanical properties were assessed by continuous stiffness measurement (CSM) nanoindentation using an Agilent G200 and a Berkovich diamond indenter at a constant loading-rate-to-load-ratio of 0.05 s^{-1}. To examine differences in indent morphology, all films were indented to the same load using a Hysitron Ti950 and imaged in scanning probe mode under a load of 2 μN with a Berkovich tip.

The compositions of all thin films are summarized in Table I. The errors are estimated from the percent error when fitting the spectra. The results demonstrate that the substrate temperature does

TABLE I. Composition of sputtered Pd-based MG thin films at different substrate temperatures as determined by EDS. The errors are determined from the percent error when fitting the EDS spectra.

Substrate temperature (K)	Pd (at. %)	Cu (at. %)	Si (at. %)
298	77.6 ± 10	6.2 ± 1.0	16.2 ± 1.7
333	78.6 ± 10	6.2 ± 1	14.6 ± 1.7
394	79.7 ± 10	5.9 ± 0.9	15.6 ± 1.6
461	78.7 ± 10	6.3 ± 1.0	15.0 ± 1.6
483	77.3 ± 10	6.5 ± 1.0	15.8 ± 1.7
553	77.5 ± 10	6.5 ± 1.0	15.9 ± 1.6

not affect the film composition, implying that all property changes reflect isochemical changes in the glass. In addition, the average film composition is $Pd_{78.3}Cu_{6.2}Si_{15.5}$, which agrees well with the target compositions of $Pd_{77.5}Cu_6Si_{16.5}$. The oxygen content was also analyzed by EDS. Given the challenges in assessing light elements by EDS, we focus on the qualitative result that most thin films appeared to have consistent oxygen content with two notable exceptions. The 298 K and 483 K deposited thin films contain approximately 100% and 50% more oxygen than the remaining thin films, respectively. Figure 1 shows structural characterization of the MG thin films. XRD patterns for thin films deposited at an actual substrate temperature of 333 K, 394 K, 461 K, 483 K, and 553 K (Fig. 1(a)) show characteristic amorphous patterns, indicated by a single diffuse peak around 40° 2θ at elevated temperatures. In contrast, the film deposited at 298 K is crystalline as indicated by the narrow peak at 40° 2θ and the secondary peak around 46° 2θ, likely corresponding to the (111) and (200) peaks from a crystalline Pd phase. Bright field TEM cross-sectional images from a thin film deposited at 298 K show many contrast features and provide clear evidence of crystallites, which supports XRD observations. This observation is also supported by the inset selected area electron diffraction pattern (SAED) (Fig. 1(b)), which shows a multitude of distinct scattering rings. In addition to the high quenching rates during deposition and limited adatom mobility, the detrimental effect of oxygen on glass forming ability[35] likely contributes to the crystallization observed in the thin film deposited at 298 K, which showed twice the oxygen content. In contrast, bright field TEM observations on a cross section of a representative glassy thin film deposited at 461 K shows that the film is featureless and the SAED pattern shows only diffuse hallows, indicating an amorphous structure (Fig. 1(c)) and corroborating the results from XRD.

Nanoindentation of MG films on Si substrates was performed using the CSM method. Depth-resolved results are shown in Figure 2. The Oliver-Pharr modulus and hardness depth profiles are
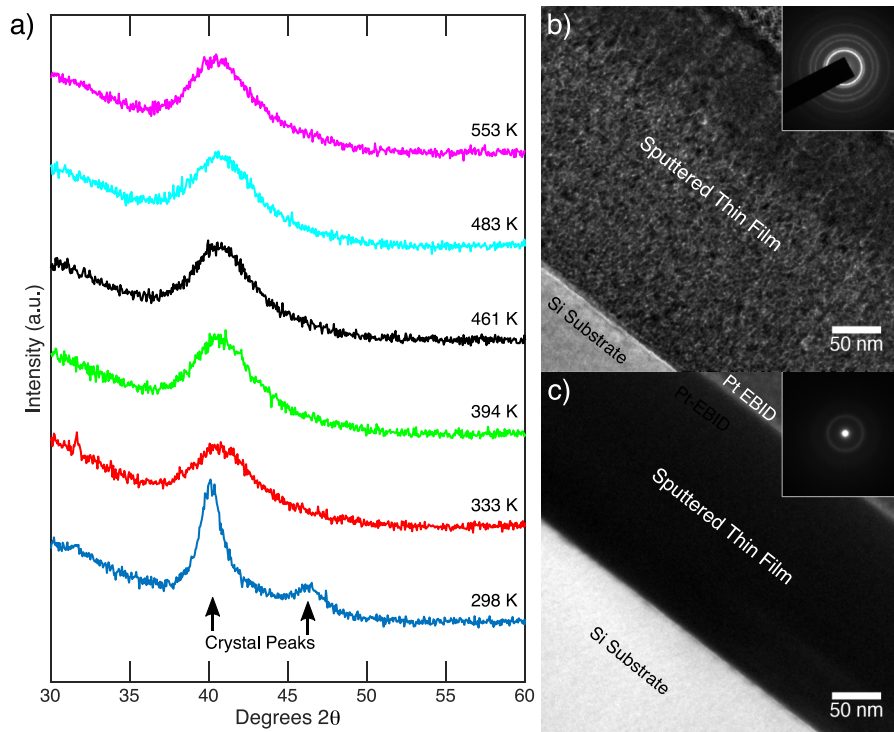

FIG. 1. (a) Structural characterization of sputtered thin films was performed by XRD. The thin film deposited at 298 K appeared crystalline as indicated by the two distinct crystal diffraction peaks, which likely correspond to the (111) and (200) peaks from a crystalline Pd phase. All other films were x-ray amorphous as indicated by the single broad diffraction peak. XRD observations were supported by TEM on the 298 K film (b) and 461 K film (c). Again the 298 K film appeared crystalline as evidenced by bright field contrast within the film and multiple sharp diffraction rings in the electron diffraction pattern (inset). The 461 K film was amorphous as evidenced by the lack of contrast within the film and diffuse halos in the electron diffraction pattern (inset).
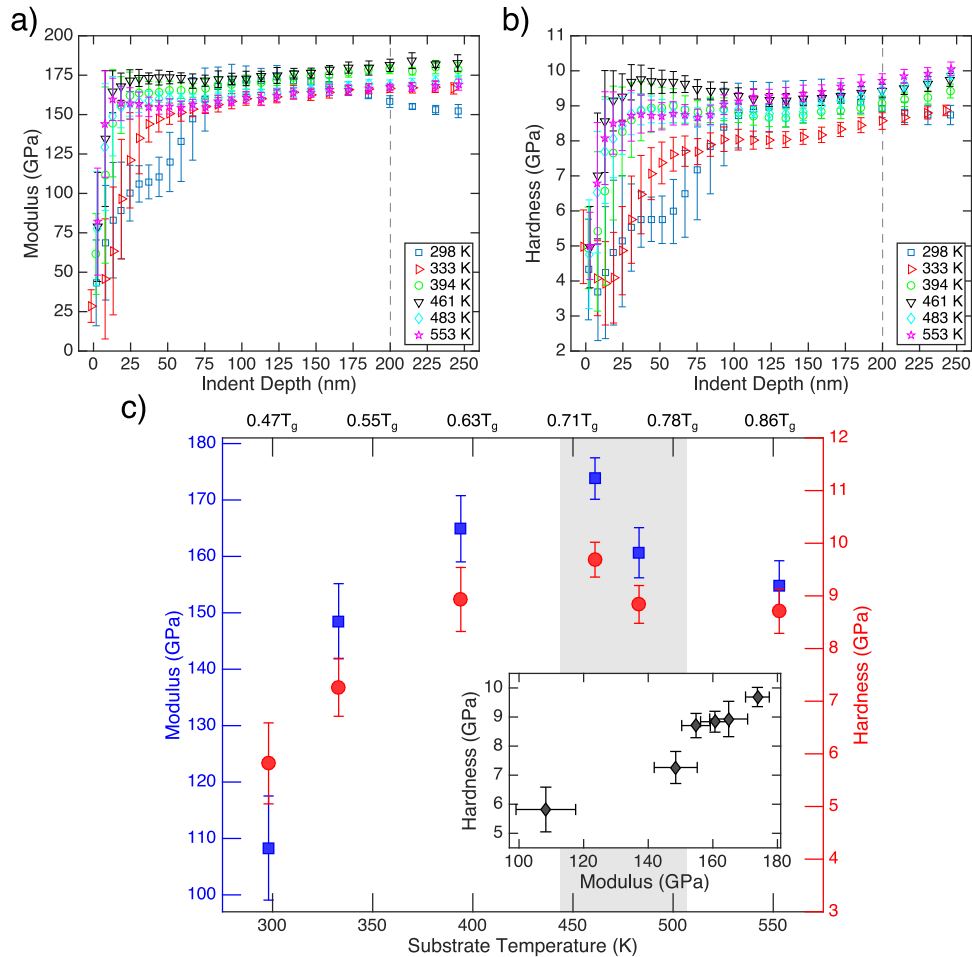
FIG. 2. Modulus and hardness were measured by nanoindentation using the continuous stiffness method. The depth profiles for modulus and hardness are shown in (a) and (b), respectively. The film properties were then determined as an average over the depth range of 45-55 nm. The resulting average mechanical properties are presented in (c) as a function of the measured substrate temperature. The error bars represent the standard deviation across the sampled depth window. Here, the inset shows the scaling of hardness with modulus.

shown in Figure 2(a) and Figure 2(b), respectively. Each point is an average of 16 indentations and the error bar is the standard deviation of the included data. The 298 K film shows a plateau in modulus and hardness at indentation depths between 25 nm and 50 nm before rapidly increasing. All other films show increasing hardness and modulus before plateauing by 50 nm for the 333 K film and 25 nm for the remaining thin films. Further analysis shows our results to be insensitive to the exact choice of the averaging window (see supplementary material for discussion).[49]

Due to the small modulus difference (∼10%) between the MG films and Si, the substrate has a limited effect on the Oliver-Pharr modulus and hardness for indentation depths smaller than 25% of the film thickness.[36,37] Furthermore, the increases in modulus and hardness at small depths (<20 nm) are likely due to the indenter tip blunting and surface roughness.[38] Additionally, we have analyzed the potential influence of pile-up during nanoindentation and estimate the error in contact area to be less than 4% for all deposition temperatures (see supplementary material for discussion).[49] Thus the potential influence of both the substrate and pile-up is substantially less than the variation in properties observed.

Accordingly, to compare the effect of deposition temperature, an average modulus and hardness are extracted by averaging over 45-55 nm of indentation depth (Figure 2(c)). From Figure 2(c) it is observed that the modulus and hardness increase with increasing deposition temperature until 461 K, indicative of an increasingly relaxed glass structure. Above 461 K, the modulus and
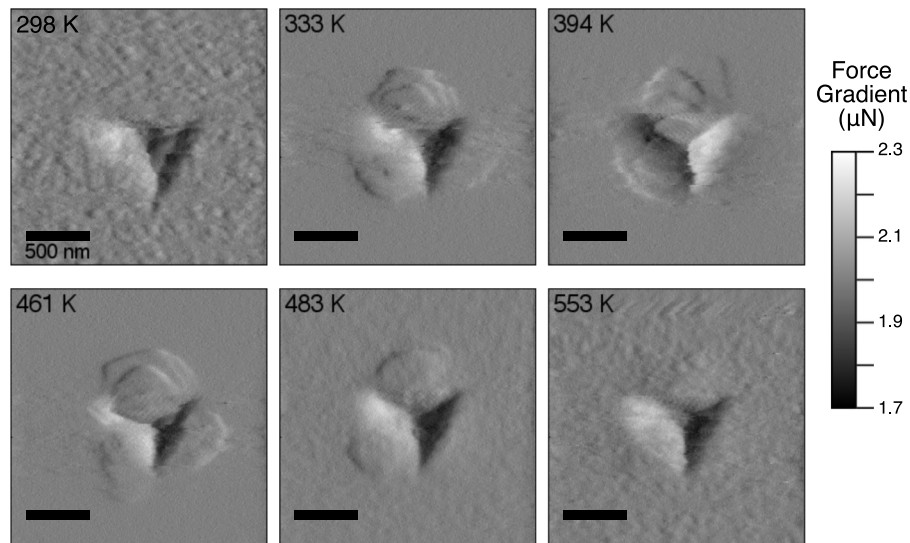
FIG. 3. Indent morphologies are observed *in situ* after indenting to 2000 μN using the scanning probe mode under an applied load of 2 μN. Here gradient force images, which are the scanning probe set point error and indicate the slope of the surface, are shown to identify changes in indent morphology. As the deposition temperature increases shear bands become more pronounced with the 461 K film showing the most distinct shear bands. Further increasing the deposition temperature results in less distinct shear bands. While interpretation of the indent morphology is complicated by potential influence of the substrate, the 461 K film showed the shallowest indent and the largest shear bands, which emphasizes its most well relaxed structure.

hardness decrease with increasing substrate temperature, suggesting more rejuvenated glasses at higher temperatures. Additionally, the inset in Figure 2(c) shows the scaling of hardness with modulus. It is expected that strength and modulus in MGs scale proportionally,[39] which is reflected in the inset.

To elucidate differences in plastic deformation mechanisms for films deposited in different structural states, the indent morphology was also observed by scanning probe imaging. Figure 3 shows gradient force images (scanning set point error) that indicate the slope of the surface and highlight local topographical features in the vicinity of the indents. Identified surface features were analyzed from line profiles taken from the height images. The 298 K film shows no pileup around the indent, indicating that no shear bands form in the crystalline film. As the deposition temperature increases shear bands are observed around the indent, primarily at the top of the impression. At 333 K, a few large shear bands are identified with an average step height difference of 10.6 nm. As the substrate temperature increases the shear bands become more pronounced and increasingly visible at the lower left edge of the indents. The thin film deposited at 461 K exhibits the largest, most distinct shear bands with an average step height of 12.6 nm. Above 461 K, the shear bands become less distinct until shear bands are poorly resolved at 553 K. However, measurement of the step heights reveals an average shear band height of 10.0 nm, which qualitatively agrees with the shear band heights at 333 K. Additionally, it is important to note that the observation of shear bands is influenced by variations in indent depth under the same applied load. Specifically, the 333 K film was indented deeper than the 461 K film potentially resulting in larger shear bands. Yet, the 461 K film showed the largest shear bands despite having the shallowest indent. Thus, while variations in indent depth influence the observation of shear bands, careful analysis reveals a qualitative transition in shear band behavior towards relatively large, distinct shear bands in the most relaxed structural state.

From the nanoindentation results, it is evident that the substrate temperature strongly influences the mechanical properties through isochemical modifications to the glassy structure. The hardness increases 33.5% from 7.26 ± 0.55 GPa at 333 K to 9.69 ± 0.33 GPa at 461 K, a difference of 2.43 GPa. Further increasing the deposition temperature decreases the hardness to 8.71 GPa at 553 K. The trends in hardness are reflected in changes in indent morphology, highlighting differences in

both the extent and mode of plastic deformation. Together, the changes in mechanical response indicate differences in glass structural state not reflected in scattering measurements (Fig. 1) and a most relaxed glass occurring at 461 K (0.73T_g for the bulk glass[40]).

To approximate the changes in structural state and develop relationships between mechanical and thermal properties, we apply a previously developed model for metallic glass strength.[20] Briefly, the mechanical energy required to initiate plasticity in a MG is equated to the thermal energy required to reach the glass transition.[41,42] This equivalence is supported by simulations, which observe a scaling relationship between temperature and glass strength.[43] By applying the model and comparing two MGs prepared in different structural states, changes in strength can be equated to changes in T_f, as $\Delta T_f = -\Delta\sigma_y V/(C_{pl} - C_{pg})$, where ΔT_f is the difference in T_f, $\Delta\sigma_y$ is the change in yield strength, V is the molar volume, C_{pl} is the supercooled liquid heat capacity, and C_{pg} is the glass heat capacity extrapolated from well below T_g.[20] Using an experimentally determined Tabor factor of $H/3.5 = \sigma_y$,[44] $C_{pl} - C_{pg} \approx 18.6$ J/mol·K,[40] and a calculated molar volume of 8.92 cm³/mol, T_f is estimated to increase by 333 K from the 333 K film to the 461 K film. Similarly, comparing the 461 K deposition to the 553 K deposition suggests that T_f decreases by 134 K by increasing the deposition temperature past the peak hardness condition. Owing to the potential substrate and indentation strain-rate effects[45] the estimated T_f changes are likely an upper bound.

Our observations that the mechanical response and structural state are controlled by substrate temperature add an additional dimension to previous studies on ultrastable organic and metallic glasses.[30–33] Recent reports investigated the structural state and kinetic stability through calorimetry; a systematic decrease in T_f and a shift of T_g to higher temperatures was observed as the deposition temperature was raised to between 0.7T_g and 0.8T_g.[30–33] Here, we make parallel observations based on measurements of the mechanical response. However, we are the first to report on the plastic response of MGs up to the ultrastable limit. We observed that the hardness significantly increases by 33.5% and shear banding becomes increasingly prevalent at 461 K. The peak in mechanical properties at 461 K (0.73T_g) falls within the expected range of temperatures for the formation of ultrastable MGs as reported by Samwer *et al.*,[33] indicated in Figure 2(c) as the shaded grey region.

Thus, the hardness results point towards the range of structural states achievable in this Pd-based MG. Here, one limit is the apparent ultrastable glass deposited at 461 K. The other observed limit is the film deposited at 333 K, which shows the lowest hardness indicating the most rejuvenated glass. The fictive temperature analysis suggests that these two extremes differ by 6.19 kJ/mol in excess enthalpy and 333 K in T_f. In comparison to previous reports on T_f and excess enthalpy differences, our results owing to different deposition temperatures are beyond the variation in T_f(~100 K) achievable through annealing,[29] and previously reported changes due to both ion irradiation and SPD in a Pt-based glass (~3 kJ/mol and ~100 K)[20] and Zr-based glasses (~4.5 kJ/mol and ~150 K).[9,46] Not only do these large differences signify large variations in glass structure beyond the limits of conventional MG processing,[6,9] the changes are encoded at the time of glass formation at temperatures and at time scales far below those necessary for post-processing structural relaxation treatments.[47]

Collectively, the mechanical property results suggest two deposition regimes, in agreement with previous reports on both organic and metallic glasses.[30,31,33] At low temperatures, below the peak modulus and hardness condition, increasing the deposition temperature produces a more relaxed structural state. At high temperatures, above the peak modulus and hardness condition, increasing the deposition temperature results in a more rejuvenated structural state. In both regimes, the resulting structure is determined by the increased surface mobility of vapor deposited adatoms as compared to atoms in the bulk.[30,31] In the low temperature regime, increasing the substrate temperature increases the surface mobility allowing adatoms to find deep positions in the PEL. In contrast, in the high temperature regime the adatoms have high mobility. As a result, the adsorbed atoms have sufficient thermal energy to overcome local energy barriers and move up the rugged PEL landscape. This suggests that the high mobility surface atoms behave similarly to the supercooled liquid,[30,31] leading to structures and properties analogous to quenched glasses.

However, we also observe that while the film deposited at 483 K (0.76T_g) lies within the expected ultrastable deposition temperature window, it exhibits a lower hardness of 8.84 GPa

compared to the 461 K film. This discrepancy could stem in part from the higher oxygen content (~50% higher than) in the 483 K film. Increased oxygen content has been linked to decreased strength[48] in metallic glasses. Regardless, differences in oxygen content do not vary systematically with deposition temperature, whereas the mechanical properties of the glassy films do. Thus, we conclude that the excess oxygen present in the two films does not contribute significantly to the overall trends in MG thin film mechanical properties.

In conclusion, we have demonstrated isochemical control over thin film MG properties by varying the deposition temperature. Rather than relying on post-processing, the structural state, mechanical properties, and deformation morphology are programmed at the time of glass formation. Based on the hardness increase of 2.43 GPa we estimate T_f to increase by 333 K, which exceeds T_f differences enacted by previously explored methods including thermal treatments, ion irradiation, and SPD. This control arises due to the different roles of enhanced surface mobility in the low and high temperature deposition regimes. Therefore, these results indicate that varying the deposition temperature during PVD enables the greatest range of glass structural states, from ultrastable to highly liquid-like, to be achieved in metallic glasses.

[1] M. Ashby and A. Greer, Scr. Mater. **54**, 321 (2006).
[2] J. Ding, Y.-Q. Cheng, and E. Ma, Acta Mater. **69**, 343 (2014).
[3] W. Li, H. Bei, Y. Tong, W. Dmowski, and Y. F. Gao, Appl. Phys. Lett. **103**, 171910 (2013).
[4] I. Gallino, M. B. Shah, and R. Busch, Acta Mater. **55**, 1367 (2007).
[5] X. Hu, S. C. Ng, Y. P. Feng, and Y. Li, Phys. Rev. B **64**, 172201 (2001).
[6] Y. Liu, H. Bei, C. T. Liu, and E. P. George, Appl. Phys. Lett. **90**, 28 (2007).
[7] G. Kumar, D. Rector, R. D. Conner, and J. Schroers, Acta Mater. **57**, 3572 (2009).
[8] S. Xie and E. P. P. George, Acta Mater. **56**, 5202 (2008).
[9] F. Meng, K. Tsuchiya, Y. Yokoyama, I. Seiichiro, and Y. Yokoyama, Appl. Phys. Lett. **101**, 121914 (2012).
[10] Q. P. Cao, J. F. Li, Y. H. Zhou, and J. Z. Jiang, Scr. Mater. **59**, 673 (2008).
[11] S. Scudino, K. B. Surreddi, M. S. Khoshkhoo, M. Sakaliyska, G. Wang, and J. Eckert, Adv. Eng. Mater. **12**, 1123 (2010).
[12] Y. Zhang, W. H. Wang, and A. L. Greer, Nat. Mater. **5**, 857 (2006).
[13] J. Fu, Y. Zhu, C. Zheng, R. Liu, and Z. Ji, Appl. Surf. Sci. **313**, 692 (2014).
[14] J. Fornell, A. Concustell, A. L. L. Greer, S. Suriñach, M. D. D. Baró, and J. Sort, J. Alloys Compd. **586**, S36 (2014).
[15] C. E. Packard, E. R. Homer, N. Al-Aqeeli, and C. A. Schuh, Philos. Mag. **90**, 1373 (2010).
[16] Y. C. C. Lo, H. S. S. Chou, Y. T. T. Cheng, J. C. C. Huang, J. R. R. Morris, and P. K. K. Liaw, Intermetallics **18**, 954 (2010).
[17] S. V. Ketov, Y. H. Sun, S. Nachum, Z. Lu, A. Checchi, A. R. Beraldin, H. Y. Bai, W. H. Wang, D. V. Louzguine-Luzgin, M. A. Carpenter, and A. L. Greer, Nature **524**, 200 (2015).
[18] R. Gerling, F. P. Schimansky, and R. Wagner, Acta Metall. **35**, 1001 (1987).
[19] R. Raghavan, K. Boopathy, R. Ghisleni, M. Pouchon, U. Ramamurty, and J. Michler, Scr. Mater. **62**, 462 (2010).
[20] D. J. Magagnosc, G. Kumar, J. Schroers, P. Felfer, J. M. Cairney, and D. S. Gianola, Acta Mater. **74**, 165 (2014).
[21] J. Gu, M. Song, S. Ni, S. Guo, and Y. He, Mater. Des. **47**, 706 (2013).
[22] Y.-Y. Zhao and X. Zhao, J. Alloys Compd. **515**, 154 (2012).
[23] J. Saida, R. Yamada, and M. Wakeda, Appl. Phys. Lett. **103**, 221910 (2013).
[24] Y. Fan, T. Iwashita, and T. Egami, Phys. Rev. Lett. **115**, 045501 (2015).
[25] Y. Fan, T. Iwashita, and T. Egami, Nat. Commun. **5**, 5083 (2014).
[26] J. Qiao, J. M. Pelletier, and R. Casalini, J. Phys. Chem. B **117**, 13658 (2013).
[27] R. Busch, J. Schroers, and W. H. Wang, MRS Bull. **32**, 620 (2007).
[28] C. T. Moynihan, A. J. Easteal, M. A. DeBolt, and J. Tucker, J. Am. Ceram. Soc. **59**, 12 (1976).
[29] G. Kumar, P. Neibecker, Y. H. Liu, and J. Schroers, Nat. Commun. **4**, 1536 (2013).
[30] K. L. Kearns, S. F. Swallen, M. D. Ediger, T. Wu, and L. Yu, J. Chem. Phys. **127**, 154702 (2007).
[31] S. F. Swallen, K. L. Kearns, M. K. Mapes, Y. S. Kim, R. J. McMahon, M. D. Ediger, T. Wu, L. Yu, and S. Satija, Science **315**, 353 (2007).
[32] Z. Fakhraai, T. Still, G. Fytas, and M. D. Ediger, J. Phys. Chem. Lett. **2**, 423 (2011).
[33] H. Bin Yu, Y. Luo, and K. Samwer, Adv. Mater. **25**, 5904 (2013).
[34] I. Lyubimov, M. D. Ediger, and J. J. de Pablo, J. Chem. Phys. **139**, 144505 (2013).
[35] W. Wang, Prog. Mater. Sci. **52**, 540 (2007).
[36] S. Han, R. Saha, and W. Nix, Acta Mater. **54**, 1571 (2006).
[37] J. Hay and B. Crawford, J. Mater. Res. **26**, 727 (2011).
[38] W. C. Oliver and G. M. Pharr, J. Mater. Res. **19**, 3 (2004).

[39] W. Johnson and K. Samwer, Phys. Rev. Lett. **95**, 195501 (2005).
[40] F. Gillessen and D. M. Herlach, J. Non-Cryst. Solids **117-118**, 555 (1990).
[41] B. Yang, C. T. Liu, and T. G. Nieh, Appl. Phys. Lett. **88**, 221911 (2006).
[42] Y. Liu, C. Liu, W. Wang, A. Inoue, T. Sakurai, and M. Chen, Phys. Rev. Lett. **103**, 065504 (2009).
[43] P. Guan, M. Chen, and T. Egami, Phys. Rev. Lett. **104**, 205701 (2010).
[44] H. S. Chen, J. T. Krause, and E. Coleman, J. Non-Cryst. Solids **18**, 157 (1975).
[45] B. Yang and T. G. Nieh, Acta Mater. **55**, 295 (2007).
[46] X. L. Bian, G. Wang, H. C. Chen, L. Yan, J. G. Wang, Q. Wang, P. F. Hu, J. L. Ren, K. C. Chan, N. Zheng, A. Teresiak, Y. L. Gao, Q. J. Zhai, J. Eckert, J. Beadsworth, K. A. Dahmen, and P. K. Liaw, Acta Mater. **106**, 66 (2016).
[47] K. L. Kearns, S. F. Swallen, M. D. Ediger, T. Wu, Y. Sun, and L. Yu, J. Phys. Chem. B **112**, 4934 (2008).
[48] R. D. Conner, R. E. Maire, and W. L. Johnson, Mater. Sci. Eng. A **419**, 148 (2006).
[49] See supplementary material at http://dx.doi.org/10.1063/1.4960388 for a complete discussion and analysis of the potential influence of pile-up.